LA-UR-19-24826 (Accepted Manuscript)

Scale Bridging Damage Model for Quasi-Brittle Metals Informed with Crack Evolution Statistics

Larkin, Kevin
Rougier, Esteban
Chau, Viet Tuan
Srinivasan, Gowri
Abdelkefi, Abdessattar
Hunter, Abigail

To be published in: Journal of the Mechanics and Physics of Solids

DOI to publisher's version: 10.1016/j.jmps.2020.103921

Permalink to record: http://permalink.lanl.gov/object/view?what=info:lanl-repo/lareport/LA-UR-19-24826

Journal Pre-proof

Scale Bridging Damage Model for Quasi-Brittle Metals Informed with Crack Evolution Statistics

Kevin Larkin, Esteban Rougier, Viet Chau, Gowri Srinivasan, Abdessattar Abdelkefi, Abigail Hunter

PII: S0022-5096(20)30157-5
DOI: https://doi.org/10.1016/j.jmps.2020.103921
Reference: MPS 103921

To appear in: *Journal of the Mechanics and Physics of Solids*

Received date: 19 July 2019
Revised date: 20 February 2020
Accepted date: 25 February 2020

Please cite this article as: Kevin Larkin, Esteban Rougier, Viet Chau, Gowri Srinivasan, Abdessattar Abdelkefi, Abigail Hunter, Scale Bridging Damage Model for Quasi-Brittle Metals Informed with Crack Evolution Statistics, *Journal of the Mechanics and Physics of Solids* (2020), doi: https://doi.org/10.1016/j.jmps.2020.103921

Highlights

- Improved effective moduli model for fracture of quasi-brittle materials
- Model informed with crack length and orientation statistics
- Stress based degradation of individual material zones
- Excellent agreement between numerical results and experimental flyer plate data

Scale Bridging Damage Model for Quasi-Brittle Metals Informed with Crack Evolution Statistics

Kevin Larkin[a,b,*], Esteban Rougier[b], Viet Chau[b], Gowri Srinivasan[b], Abdessattar Abdelkefi[a], Abigail Hunter[b,*]

[a]New Mexico State University Department of Mechanical and Aerospace Engineering, Las Cruces, NM 88003, USA
[b]Los Alamos National Laboratory, Los Alamos, NM 87545, USA

Abstract

Computationally efficient methods for bridging length scales, from highly resolved micro/meso-scale models that can explicitly model crack growth, to macro-scale continuum models that are more suitable for modeling large parts, have been of interest to researchers for decades. In this work, an improved brittle damage model is presented for the simulation of dynamic fracture in continuum scale quasi-brittle metal components. Crack evolution statistics, including the number, length, and orientation of individual cracks, are extracted from high-fidelity, finite discrete element method (FDEM) simulations and used to generate effective material moduli that reflect the material's damaged state over time. This strategy allows for the retention of small-scale physical behaviors such as crack growth and coalescence in continuum scale hydrodynamic simulations. However, the high-fidelity simulations required to generate the crack statistics are computationally expensive. Thus, steps were taken to produce a flexible constitutive model to reduce the number of costly high-fidelity simulations needed to produce accurate results. A new stress based degradation criterion is introduced for the degradation of individual material zones. This allows for the development of a heterogeneous damage distribution within the bulk material. Then a flow stress model is added to the hydrodynamic simulation to account for plasticity in quasi-brittle materials. As a result, the effective moduli model can be applied to a larger range of materials. The effective moduli constitutive model is used to simulate beryllium flyer plate experiments. The results from the continuum scale simulations using statistics from a single high-fidelity simulation are found to be in excellent agreement with numerical and experimental velocity interferometer data. The same set of crack statistics are used to extrapolate the results of a higher rate flyer plate case using the effective moduli model. The extension of this model to higher rate cases shows promise for further reducing the number of costly high-fidelity simulations needed to generate crack statistics.

Keywords:
brittle fracture, shock loading, effective elastic moduli, crack statistics, finite-discrete element method

1. Introduction

Often, brittle fracture is the primary cause of material failure in dynamic loading scenarios. As, brittle failure often occurs suddenly (on relatively short time scales), it is very difficult to accurately predict especially under high-rate loading conditions, which only further shorten the time scales associated with the growth, coalescence and interactions of micro-cracks. However, there are many applications that require such predictive models. For example, models for dynamic brittle fracture have recently been developed for geomechanics applications such as blasting or percussive drilling (Saadati et al., 2016; Cho et al., 2003), ballistic impacts of ceramic plates for vehicle or body armor (Krishnan et al., 2010; Chen et al., 2007), and general crack growth in quasi-brittle materials (Saksala et al., 2015). Quasi-brittle materials, often metals, can add further difficultly since the overall material behavior changes dramatically from

*Los Alamos National Laboratory
PO Box 1663 MS T086
Los Alamos, NM 87545, USA
ahunter@lanl.gov, klarkin@lanl.gov

ductile to brittle with an increase in the applied loading rate (Blumenthal et al., 1998). Beryllium is an example of a quasi-brittle metal that is a highly desirable for many industrial applications in the automotive, aerospace, and defense industries because of its high strength to weight ratio (Kolanz, 2001). However, the high-rate loading conditions materials undergo during fabrication and during the applications themselves lead to the growth and coalescences of micro-cracks, prompting abrupt material failure that is extremely difficult to predict. The lack of predictive models addressing the abrupt failure of these materials at a component level drastically limits their real-world applicability despite their attractive material properties.

Over the years, several methods bridging a range of length scales have been developed and applied to the growth of crack networks within brittle materials, including molecular dynamics simulations (Dienes and Paskin, 1987), peridynamics (Silling and Askari, 2005), phase field approaches (Ambati et al., 2015), the extended finite element method (XFEM) (Zi and Belytschko, 2003), and the finite discrete element method (FDEM) (Munjiza et al., 1995). On the atomistic and meso-scales, these approaches can finely resolve crack growth, propagation, interaction, coalescence, etc., and the physics that drive these processes. However, these frameworks are relatively limited in time and length-scales such that they cannot address material failure at the component-scale (cm and larger). Larger length scale approaches, such as XFEM and FDEM, can produce highly resolved micro-scale simulations that discretely model individual cracks, producing accurate predictions of crack network evolution. However, the highly resolved mesh needed for these models results in extraordinarily high computation costs when modeling continuum-scale systems. A common method for reducing the computational costs while retaining micro-scale physical phenomena are concurrent and serial multi-scale methods (Horstemeyer, 2009; Zhou and Chen, 2018). Concurrent multi-scale methods commonly use finite elements to model far field effects while molecular dynamics and/or quantum mechanics is used to model regions were cracks are formed (Tadmor et al., 1996; Abraham et al., 1998; Rudd and Broughton, 1998; Lee et al., 2009; Li et al., 2010). These types of multi-scale methods have recently been used to study the properties of systems with one or very few micro-cracks in small continua (Xu et al., 2017; Qiu et al., 2018). However, using this type of scale bridging technique can become computationally expensive when modeling large systems with dense, uniformly distributed crack networks, such as machine components.

Converse to these highly-resolved and lower length-scale methods, continuum-scale constitutive models can model the overall material response for large samples with relative computational ease. Such models have been developed over several decades, and there has been much effort in the development of more physical informed constitutive models, particularly for systems undergoing dynamic loading conditions (Addessio and Johnson, 1990; Camacho and Ortiz, 1996; BaÅant et al., 2000; Ayyagari et al., 2018; Zubelewicz et al., 2014). However, in order to operate at these larger length-scales, major assumptions about a material's microstructure and active deformation mechanisms are inherent to these formulations in order to homogenize the system up to the scale of interest. Of particular importance to the problem of brittle damage and failure, key assumptions include generalizations of the distribution, geometry, and orientation of the cracks within a body and their subsequent evolution. Because the features that guide crack evolution are often on a scale that is orders of magnitude lower than that of the materials system of interest, the discrete nature of the cracks themselves is typically lost. While such assumptions are necessary to remain at a large length scale, it becomes very difficult to capture key physics driving the evolution of micro-cracks within the body, and hence it is also difficult to accurately predict the corresponding material response.

Consequently, serial multi-scale approaches have evolved. These methods use information from separate micro-scale analyses to inform a macro-scale model through statistical analysis or a homogenization scheme used to find the effective properties of the damaged material (Ju and Tseng, 1992; Ju and Chen, 1994a,b; Ju and Tseng, 1995; Margolin, 1984; Kushch et al., 2009; Gailly and Espinosa, 2002; Sheng and Zeng, 2016; Vaughn et al., 2019). These methods have developed from traditional effective medium frameworks (Zimmerman, 1985; Kachanov, 1993; Budiansky and O'Connell, 1976; Horii and Nemat-Nasser, 1983; Hashin, 1988; Margolin, 1983), which account for damage accumulation through the degradation of a material's elastic moduli over time, resulting in the determination of an "effective moduli". These multi-scale approaches intend to retain more information about the evolution of the crack network by including statistical information about the changing crack lengths and orientations. Often simplified crack distributions, such as randomly oriented or parallel cracks, are studied because they allow for some degree of analytic tractability (Ju and Chen, 1994b; Ju and Tseng, 1995; Kushch et al., 2009). Capturing the vast array of arbitrary crack configurations is still difficult, particularly when considering how the crack network evolves under loading. Under load an initially uniform distribution of cracks can become quite heterogenous, particularly when dynamic loading is considered. It has been demonstrated that microstructural defects such as voids, micro-cracks, and inclusions have a significant effect on a material's dynamic strength (Saadati et al., 2016; Sheng and Zeng, 2016; Abedi et al., 2017). Moreover, every material sample has a unique microstructure which contains different numbers, types, and severities of defects. For this reason, statistical methods for analyzing crack formation are needed to represent a wide range of possible defect distribution cases and produce a realistic representation of the average material behavior.

In this work, the advantages of serial multi-scale modeling techniques are leveraged to create an efficient and accurate representation of evolving crack networks under dynamic loading conditions within quasi-brittle metals. A high-fidelity model that can resolve discrete cracks is used to generate statistical information about the crack network such as, the number of cracks, crack length and crack orientation over time. These statistics are then used to inform an effective moduli constitutive model. Because the crack statistics in this approach are informed using a higher fidelity model, random configurations (e.g., homogeneous and/or heterogeneous) can be considered within this framework. We discuss the number of high-fidelity simulations necessary to create a statistically relevant data set in comparison to previous work directed at low-rate loading conditions (Vaughn et al., 2019). Furthermore, we investigate the ability of the continuum scale model to extrapolate higher rate loading cases. This can also reduce the need for additional statistics from computationally expensive high-fidelity simulations. Furthermore, this model accounts for plasticity in addition to the degradation of the material due to brittle damage mechanisms. Quasi-brittle metals are much more ductile than other brittle materials such as ceramics, glasses, and geo-materials, therefore, plastic deformation of the material must be included in order to accurately reproduce experimental results.

We use this model to simulate beryllium flyer plate impact experiments, with direct comparison to both numerical and experimental results. During low-rate loading, brittle failure will occur when the single weakest (largest) defect or micro-crack begins to grow and coalesce with other neighboring cracks, if present, until one dominant crack path is formed. Conversely, high-rate loading conditions cause multiple micro-cracks in a region of high stress to rapidly grow and coalesce, forming a heterogenous region of damage with many branching crack paths. In flyer plate experiments, which apply planar shock waves, this heterogeneous region of damage is typically well-defined in the test sample and called a spall region (Meyers and Aimone, 1983). The near instantaneous formation of a spall region resulting in material failure is accounted for in our approach by using a multi-element simulation in which individual elements are degraded based on the magnitude of their experienced tensile stress.

This work continues as follows: In Section 2 the statistically informed effective moduli model for quasi-brittle metals is described. Then the method for extracting crack evolution statistics from high-fidelity models for use in a continuum model is presented in Section 3. Next, in Section 4 the integration of the effective moduli model into a multiphysics hydrocode for continuum scale analysis of the fracture of quasi-brittle metals is introduced. Later, in Section 5 the results from the effective moduli model are compared with those from the high-fidelity simulation and experimental results, the effect of variations in the crack statistics is analyzed, and the ability of the model to extrapolate a higher rate loading scenario is investigated. Finally, some concluding remarks are drawn in section 6.

2. Effective moduli model formulation for statistically evolved damage

In this work, the micro-scale behavior of crack propagation is represented in a macro-scale continuum through the degradation of the material's effective moduli, calculated using the effective moduli model first proposed by Ju and Chen (Ju and Chen, 1994a,b), which is briefly described here. The effective moduli model relies on the number, length, and orientation of micro-cracks to produce probability density functions (PDFs) that describe the evolution of the crack length and orientation over time. The PDFs are then used to degrade the compliance tensor as shown in the following equations (Ju and Chen, 1994a,b):

$$S_{eff} = S^0 + S^1 + S^2 \tag{1}$$

$$S^1 = \frac{\pi(1-\nu^2)}{E} f(x) \int_\alpha \int_\Theta a^2 M_0 f(a,\theta) d\theta da \tag{2}$$

$$S^2 = \frac{\pi(1-\nu^2)}{E} f^2(x) \int_\alpha \int_\Theta a^2 M^2(a,\theta) d\theta da \tag{3}$$

where S_{eff} is the effective compliance tensor, S^0 represents the pristine compliance tensor of the material, S^1 is a damage tensor that accounts for the growth and coalescence of individual cracks in the material over time, S^2 denotes an additional damage tensor that represents the interaction of two adjacent non-intersecting cracks, a represents the crack radius, and θ is crack orientation. These two damage tensors act as corrections to the pristine compliance tensor due to the presence of micro-cracks (S^1), and their subsequent interactions (S^2). The local coordinates of the cracks are related to the global coordinate system through transformation matrices M_0 and M. Finally the material is assumed to be elastically isotropic, hence ν is Poisson's ratio, and E is Young's modulus. For a detailed derivation of equations (1-3) see Ju and Chen (1994a,b).

In the original formulation, the crack distribution within the material is assumed to be uniform, thus, removing the damage's dependance on x (Ju and Chen, 1994a). Therefore the function $f(x)$ can be replaced by the number of cracks per unit area or crack density, n. In this work, the crack radius and crack orientation are considered as independent variables, as a simplification. Therefore, $f(a, \theta)$ becomes $f(a)f(\theta)$. The damage caused by pairwise crack interactions, S^2 is negligible if the crack density is sufficiently small. However, the degradation of the material moduli due to crack interactions is removed for simplicity, and its inclusion within the framework is subject of future work. It should be noted that equations (1-3) are formulated for a material of infinite domain. This means that material fracture will never occur. Instead the effective moduli of the system will reach some constant minimum over time. However, in a finite domain, fracture can occur resulting in a material domain with no stiffness. To resolve this issue, a length scale parameter is added to the compliance degradation function, following the work of Vaughn *et al.* (Vaughn et al., 2019), to account for a finite domain. After the above simplifications the new expression for the effective compliance tensor becomes:

$$S_{eff} = S^0 + S^1_f \tag{4}$$

$$S^1_f = \left(\frac{L}{L - 2\bar{a}}\right) \frac{\pi(1-\nu^2)n}{E} \int_\alpha \int_\Theta a^2 M_0 f(a) f(\theta) d\theta da \tag{5}$$

where L denotes the length of the target plate and $\bar{a}$ is the half length of the projection of the longest crack in the direction of failure. In the case of a flyer plate, $2\bar{a}$ will approach the length of the target plate, causing S_{eff} to trend towards infinity, resulting in a fractured material with no strength. Once the degraded compliance tensor has been determined, the stress state of the material can be calculated using Hooke's Law:

$$\sigma = C_{eff}\epsilon = (S_{eff})^{-1}\epsilon \tag{6}$$

where ϵ is the elastic strain tensor and C_{eff} represents the effective stiffness tensor.

3. Generation of crack propagation statistics utilizing the Hybrid Optimization Software Suite

The continuum model presented in Section 2 relies on statistical information including the length, orientation, and evolution of individual cracks to represent damage within the material domain. In this work, information about the propagating crack network is obtained from high-fidelity simulations completed with the Hybrid Optimization Software Suite (HOSS), which is an implementation of the combined finite-discrete element method (FDEM) (Rougier et al., 2013b; Knight et al., 2013; Rougier et al., 2013a). Advantageously, this model evolves discrete cracks along element edges, and can accommodate complex crack network evolution, catastrophic failure, and even fragmentation. Here we briefly describe how damage is modeled within HOSS, however more extensive reviews detailing the model are available (Munjiza et al., 1995; Munjiza, 2004; Munjiza et al., 2012, 2015). In addition, the primary algorithms in HOSS addressing the contact interaction and finite strain elasticity formulation have also been documented (Munjiza et al., 2012, 2015).

To accurately model damage evolution, failure, and fragmentation, the FDEM divides the global system into discrete solid domains, which are then further discretized into finite elements. Each of these finite elements are connected by a user-specified number of cohesive points, modeled as non-linear springs, between the edges of finite elements (Godinez et al., 2019; Osthus et al., 2018). For all HOSS simulations presented here, four normal and four shear cohesive points are utilized; a number that has been shown to provide accurate results at reasonable computational expense (Rougier et al., 2014). These points allow the edges of the finite elements to separate under sufficient tensile and/or shear loading. Once the separation value reaches a critical value, the cohesion between the elements fails and a crack forms along the element edge. A damage parameter, D_{HOSS}, that corresponds with the severity of the element separation is determined for each element edge. D_{HOSS} ranges from 0, an undamaged edge, to 1, a fully separated edge. In this way, HOSS is able to capture crack nucleation, growth, and coalescence within the specimen over time, as it was demonstrated in previous studies (Euser et al., 2019, 2018; Rougier et al., 2014). Since discrete cracks propagate along element edges in the FDEM, a highly resolved mesh is needed to capture complex crack behavior, such as interactions between cracks and crack branching or bending behavior. Consequently, HOSS simulations can be extremely computationally expensive when modeling large components or long time scales.

In this effort, crack propagation within a flyer plate setup consisting of a beryllium target plate and a beryllium impactor (Be-Be) is analyzed. Flyer plate simulations are set up in HOSS to mimic an experiment conducted at Los Alamos National Laboratory (LANL) on samples of S200-F beryllium (Cady et al., 2012). An example of this setup as modeled in HOSS is presented in Figure 1 where h_i and h_t are the thicknesses of the impactor and target plates, respectively. The flyer plate is given an initial velocity of $v = 0.0721 cm/\mu s$. Once the flyer plate impacts the target, it creates a compressive shock wave that propagates through the target plate. When the compressive shock front reaches the back side of the target plate it reflects as a consequence of its interaction with the free surface. The returning wave then interacts with the rarefaction from the initial shock pulse creating a region of high tensile stress, normal to the plate's surface. The high tensile stress causes the micro-cracks near the mid-plane of the target plate to rapidly grow and coalesce in a direction perpendicular to the applied velocity, forming the spall region. Despite the flyer plate providing an initial compressive load, the experiment allows for the evolution of an indirect tensile load that results in the evolution of damage due to crack opening. Eventually, a dominant horizontal crack within the spall region will span the length of the target plate leading to Mode I failure.

In the HOSS simulation set-up, $h_i = 2mm$, $h_t = 4mm$, and the diameter of the impactor and target plates is 28.8mm. The target plate initially contains 200 micro-cracks between 0.1 and 0.3 millimeters in length. The position of each crack within the target plate is determined through random sampling of a uniform distribution. Similarly, crack orientations are determined through random sampling of a uniform distribution function constrained between the angles of -90 and 90 degrees. Crack lengths are randomly sampled from the following a power law distribution:

$$f(a) = \frac{g a^{(g-1)}}{b^g - c^g} \tag{7}$$

where c is the shortest initial crack length, b is the longest initial crack, and parameter $g = -3$. Very fine time steps of $1e^{-}5$ microseconds are required to accurately capture the rapid evolution of the crack network in HOSS. Every 250 time steps: stress, velocity, and crack evolution data is output from HOSS. A total of 480 HOSS outputs were created per simulation. The run time for each simulation was 2.5 hours on 64 processors. One hundred simulations of this type were conducted in HOSS to create a statistically relevant data set for crack network analysis. However, in each simulation the pre-existing crack network is perturbed so that the exact locations and lengths of the 200 cracks are different, thus changing the initial crack network configuration.

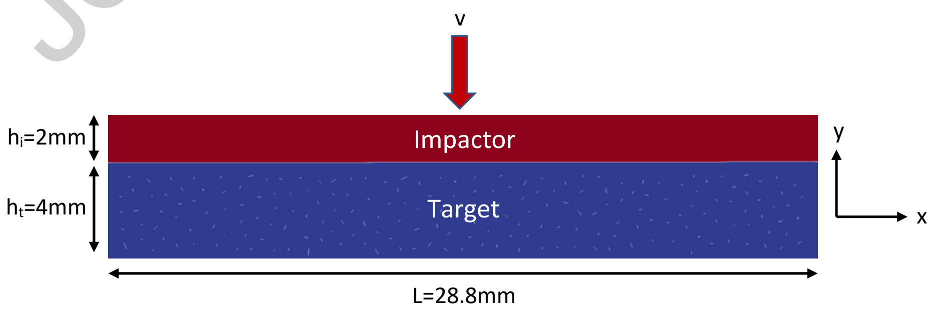

Figure 1: Initial setup of a 2D Be on Be flyer plate simulation with 200 randomly positioned and oriented micro-cracks in the target plate

The realistic crack network generated by the HOSS simulations contain complex systems of branching and turning cracks. However, the effective moduli model discussed previously in Section 2 assumes that all cracks in the domain are straight with an easily definable orientation. A reliable method for determining the length and orientation of individual cracks must be instituted to compile statistical crack information provided by HOSS so that it is usable in the effective moduli model. This requires a clear definition of how to measure a crack's length as it propagates, bends, coalesces, etc. One logical method, which we chose to apply here, is to identify the right-most and left-most points of a crack and use the straight line distance between these points as the crack length (i.e. the Euclidean length). Then the angle between this straight line and the horizontal axis can be used as the crack orientation. We note, however, that one could think of many possible ways to define a crack's length and subsequent orientation. Previous work by Vaughn *et al.* (Vaughn et al., 2019) utilized a similar model framework as in this work, however applied to low-rate tensile loading of geomaterials (concrete). In this work, they investigated various definition of the crack length including the projection normal to the applied load, Euclidean length, and the total crack length. They found that the Euclidean length measurement technique yielded the best results when compared to the other crack length definitions for the effective moduli model, hence, we have also chosen to use this length measure in the analysis presented here.

A Python script was used to identify the left and right most points of every crack in each HOSS output. Then the Euclidean length and resulting orientation of each crack was calculated using the extracted data. Consequently, PDFs of crack length and orientation can be generated for each HOSS time step. Then crack data at every time step for all 100 HOSS simulations can be combined into one statistically significant data set, if necessary. Example crack length and orientation statistics generated from a single HOSS simulation are presented in Figures 2 and 3, respectively. Significant crack growth occurs when the target plate is under tensile loading and the spall region develops. This occurs after the initial shock wave has reflected off the backside of the target plate. Hence, Figure 2 shows that little to no crack growth occurs during the compressive loading regime, before the shock is reflected. For the flyer plate statistics shown in Figure 2, a single crack within the spall region spans the width of the target plate after time, $t = 0.7425\mu s$. From analysis of Figure 3, crack orientations do not change significantly throughout the simulation. Indeed, most of the pre-existing cracks in the target plate do not grow or coalesce resulting in only minor changes in the orientation and length distributions. However, after a tensile region is formed within the target plate, cracks near the mid-plane join to form a dominant crack system that is normal to the applied loading (nearly horizontal in this case). Thus, crack orientation slightly trends towards $0°$ after fracture occurs, regardless of the initial crack distribution. An effective compliance tensor for each HOSS output can be obtained by numerically integrating Equations 4 and 5, using the crack length and orientation distributions, like those presented in Figures 2 and 3, as functions $f(a)$ and $f(\theta)$.

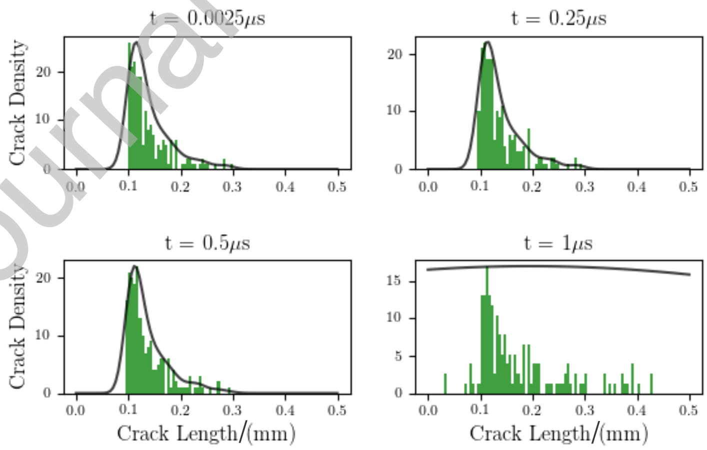

Figure 2: Crack length distributions extracted from a single HOSS simulation at various time steps. The black line represents the probability density function determined using a Gaussian kernel-density estimation

3.1. Removing time dependency for multi-zone simulations

As stated previously, statistical distributions can be generated for each HOSS output, producing a time series of statistical information. However, the effective moduli model presented in Section 2 will not be run in HOSS, but in a hydrodynamic model framework (discussed in more detail in Section 4). Hence, the problem of correlating damage

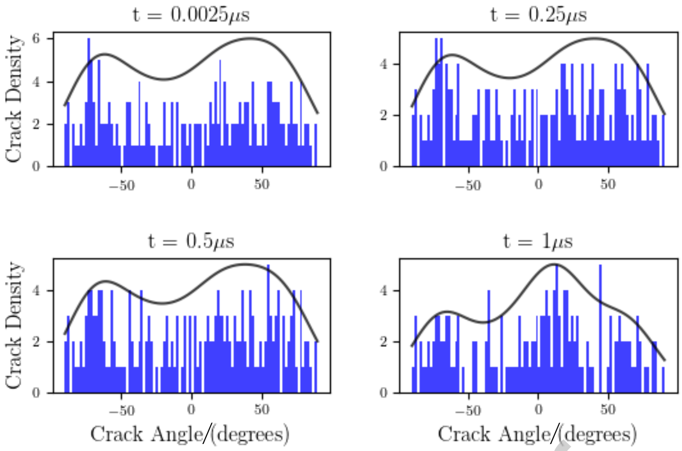

Figure 3: Crack orientation distributions extracted from a single HOSS simulation at various time steps. The black line represents the probability density function determined using a Gaussian kernel-density estimation

evolution to the simulation time step across very different codes and model implementations arises. In particular, the crack length and orientation statistics generated using HOSS output must be utilized in the effective moduli model at the appropriate point (time) in the system's damage evolution. This requires that the time step used for generating the statistics (i.e., the HOSS time step), must directly correspond to the time step used in calculations with the effective moduli constitutive model to avoid interpolation between statistical sets. Such criteria can be quite limiting, particularly if this requires statistical output from HOSS that is highly resolved in time thus, increasing data storage requirements and computational costs. These criteria could also require that the continuum-scale model be run at time steps much more resolved than typically necessary, reducing the computational efficiency gained by increasing the model's length-scale. Additionally, if we consider a system containing multiple material zones, some zones may experience much more damage than others. For example, in the case of the flyer plate experiment, the spall region near the mid-plane of the target plate is the only region that accrues large amounts of damage. Therefore, zones across the entire target plate cannot be degraded evenly over time but must be degraded individually based on some criteria determined by the applied loading or material state.

Cracks grow when a sufficient stress concentration at the crack tip causes the crack to open and spread (Griffith, 1921). Information concerning the evolution of the stress state can be extracted from HOSS's high-fidelity simulations in addition to the statistical information about the crack network. Since the spall region is generated from a tensile stress state in the target material, the maximum tensile stress within the target material domain is chosen as it is the key indicator of Mode I type damage initiation and evolution. For other loading conditions, a different metric of the stress state within a material zone may be a better indicator of damage initiation (e.g., a maximum shear stress, or an effective stress measure for combined loading conditions). Figure 4 shows the value of the maximum tensile stress in the direction of the applied loading plotted with the velocity calculated at the back of target plate over time with HOSS. The maximum tensile stress is taken to be the maximum tensile stress in any element of the HOSS simulation. For the case of the flyer plate, the maximum tensile stress occurs in elements within the spall region, however, it may not be the same element for every HOSS output . Clearly, the maximum tensile stress and velocity follow a similar trend. This, coupled with the expectation of Mode I failure, makes the maximum tensile stress a logical choice for a damage evolution criteria. The maximum tensile stress for each HOSS output is coupled with the degraded compliance tensor produced for the same HOSS output time. The maximum tensile stress value is then used as a pointer to indicate the appropriate damage tensor for a zone in the continuum model, which allows a non-homogeneous damage distribution to evolve within the target material. More details on this approach can be found in Section 4.2.

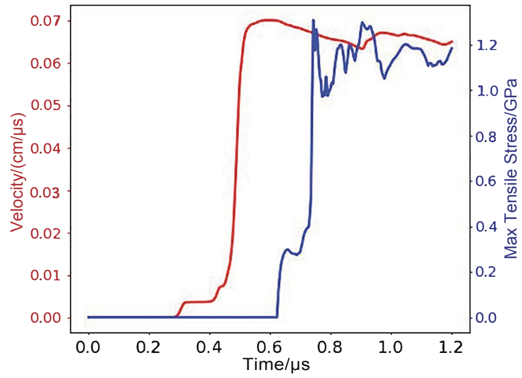

Figure 4: Maximum tensile stress in any zone in the target sample and the velocity at the rear center of the target plate over time from a single HOSS simulation.

4. The effective moduli material model in FLAG

LANL's hydrodynamic modeling software (hydrocode), FLAG, is used to perform the continuum-scale simulations. FLAG (Burton, 1992, 1994b,a) has been developed and maintained at LANL over several decades, and hence has a diverse set of modeling capabilities for solving fluid and solid mechanics problems. FLAG is a multidimensional (1D, 2D, and 3D), multiphysics research code, that uses a finite-volume approach to compute solutions using either a cell-centered or staggered-grid hydrodynamics algorithm. It utilizes an arbitrary polyhedral mesh arranged on an unstructured grid to resolve multidimensional single material, mixed material, or multi-material domains. Adaptive mesh refinement (AMR) and arbitrary Lagrangian-Eulerian (ALE) relaxation are available for mesh refinement and adaptivity in dynamic simulations. In addition, FLAG includes a wide-ranging library of models that can account for material behaviors under extreme loading conditions, and also capabilities such as slide surfaces for addressing discontinuous meshes.

FLAG has been extensively validated for a wide range of classical test problems such as the Noh, Sod shock tube, Taylor-Green vortex, and Howell problem (Burton et al., 2018). Recently, Caldwell *et al.* (Caldwell et al., 2018) performed a verification and validation study for impact cratering simulations in FLAG and found that FLAG was capable of capturing shock dynamics with relatively low error when compared to experimental results. Furthermore, this study included a comparison of results to eight other hydrocodes with similar frameworks and a mesh convergence study. Results showed that FLAG had lower deviations in solutions in comparison to analytical solutions. FLAG has been used for a wide variety of research endeavors including ejecta and transport modeling (Fung et al., 2013), turbulence modeling (Denissen et al., 2012), detonation shock dynamics (Aida et al., 2013), and material damage modeling (Tonks et al., 2007; Vaughn et al., 2019). In this work FLAG is used to simulate crack propagation in 1D and 2D flyer plate experiments using a pure Lagrange solution technique.

4.1. Integrating plasticity into the effective moduli model

While some brittle materials such as ceramics or geo-materials have negligible plasticity, quasi-brittle metals, have some ductile behavior. Additionally, the high rate loading conditions of interest here will produce compressive and tensile stresses in excess of the material's yield strength. Consequently, a plasticity model must be included to obtain an accurate result. FLAG has several built in plasticity models including von Mises plasticity, Steinberg-Guinan (Steinberg et al., 1980), and Preston-Tonks-Wallace (PTW) (Preston et al., 2003). In this case, we have chosen to use the Steinberg-Guinan flow stress model, however, any flow stress model could be used with effective moduli constitutive model using the methodology described below. It is worth noting, that the Steinberg-Guinan model (and other common flow stress models, such as PTW) assumes elastic isotropy. The Steinberg-Guinan parameters for Beryllium (Steinberg, 1996) can be found in Table 1.

In order to include the plasticity model, the total stress tensor is first split into deviatoric and volumetric components:

$$\sigma_{ij}^{0} = \sigma'_{ij} - P\delta_{ij} \tag{8}$$

where σ^0 represents the pristine stress, σ' is the stress deviator, P denotes the pressure, and δ_{ij} is the Kronecker delta function. The framework in FLAG utilizes this type of decoupling to determine the stress state in a zone, rather than using Hooke's Law directly. Hence, an equation of state (EOS) is then used to determine the zonal pressure, temperature, and the material's bulk modulus. FLAG's material library has access to both analytic and tabular EOS. In this work, we have chosen to use a tabular EOS from the SESAME database (Lyon, 1992).

The deviatoric stresses, and corresponding amount of plastic strain, of the undamaged material are determined using an isotropic radial return algorithm (Simo and Hughes, 2006). As mentioned above, the yield criterion is given by the Steinberg-Guinan model. In addition, the Steinberg-Guinan shear modulus model was used to account for temperature and pressure dependent changes in the material's shear modulus during loading. FLAG is a velocity driven code, so the elastic strains can be determined assuming an additive decomposition of the total strain:

$$\epsilon = \epsilon^{tot} - \epsilon^{p} \tag{9}$$

where ϵ is the elastic strain, ϵ^{tot} denotes the total strain, and ϵ^p represents the plastic strain. The determination of the elastic strain is the key term that accounts for plasticity in the determination of the stress state of the damaged material. In order to determine the stress state of the damaged material using the effective moduli model, the stress tensor cannot be decoupled as in Equation 8. Rather, the corrected stress tensor that includes damage must be determined for each zone directly using Hooke's Law as follows:

$$\sigma = (C^0 + C^1)\epsilon \tag{10}$$

where σ represents the stress tensor of the damaged material zone, and ϵ is calculated using equation 9. C^1 is the damage tensor that is calculated in FLAG using crack statistics from HOSS. The C^1 damage tensor is determined as follows:

$$C^1 = (S_{eff})^{-1} - C^0 \tag{11}$$

where S_{eff} has been defined previously in Equation 4 and C^0 represents the stiffness tensor of the pristine material.

Table 1: Steinberg-Guinan model parameters for Beryllium (Steinberg, 1996)

Parameter	Description	Value
ρ_0	reference density	$1.845 g/cm^3$
G_0	initial shear modulus	$1.51 Mbar$
Y_0	initial flow stress	$0.0033 Mbar$
Y_{max}	max work hardening	$0.0131 Mbar$
β	work hardening parameter	26
n	work hardening exponent	0.78
A	pressure dependence multiplier	0
B	temperature dependence multiplier	0
q_y	flow stress pressure dependence factor	1.0
f_g	melt shaping for shear modulus	0
f_y	melt shaping for flow stress	0
ρ_{0s}	crushed-up density	$1.845 g/cm^3$

4.2. Statistically informed damage evolution in FLAG

The effective moduli model in FLAG relies on the maximum tensile stress from the high-fidelity HOSS simulations to determine the appropriate crack length and orientation statistics to use to calculate the damage tensor for each zone at each time step. For the first occurrence of tensile loading in a zone σ^0 is matched to a corresponding HOSS stress value and the associated crack length and orientation statistics. If the stress value from FLAG lies between two maximum tensile stress values from HOSS, linear interpolation is used to correct the components of the computed damage tensor to provide a more accurate damage estimation. Once damage has been initiated, the pristine stress will largely overestimate the stress state within the damaged material because energy released by crack growth is not accounted for in the calculation of the pristine stress. Thus, for subsequent iterations, a trial stress is calculated to estimate the stress in each damaged zone as follows:

$$\sigma^T = (C_n^0 + C_{n-1}^1)\epsilon_n \qquad where: \epsilon_n = \epsilon_n^{tot} - \epsilon_n^p \tag{12}$$

where σ^T represents the trial stress and subscript n is the current time step. The trial stress is determined by first calculating the elastic strain from the pristine material conditions for the current iteration. Then the damage tensor from the previous iteration, C_{n-1}^1, is used to degrade the pristine stiffness tensor. A component of the trial stress or equivalent stress measure, such as a principle component of the trial stress, is compared to tensile stress values from HOSS and an updated set of crack statistics are obtained for the current iteration. In this work, the σ_{22}^T component of the trial stress is compared to the maximum tensile stress values from HOSS because tensile stress in the y-direction is the primary mechanism contributing to the formation of the spall region in the target plate. Finally, the corrected stress for the current damage state, σ, is calculated using the updated damage tensor as in Equation 10. A damage parameter is integrated into the effective moduli model in FLAG as a way to represent the extent to which a material zone is damaged. The damage parameter in FLAG, D_{FLAG}, has a range from zero, an undamaged zone, to one, a failed zone with no strength. The damage is determined as follows:

$$D_{FLAG} = 1 - \frac{C_{norm}^0 - C_{norm}^1}{C_{norm}^0}. \tag{13}$$

The C_{norm}^0 and C_{norm}^1 represent the components of the pristine stiffness tensor and damage tensor in the direction of loading primarily responsible for crack growth. Assuming a Mode I type failure; the tensile load will be normal to the direction of crack growth. In this work, the C_{22}^0 and C_{22}^1 components are used to calculate the damage in the target plate. When a zone in FLAG reaches a damage value, $D_{FLAG} = 1$, it is considered completely failed. The stress value in the failed zone is set to zero and failed zones cannot regain strength. This may not be appropriate for cases of cyclic loading where cracks may be closed by compressive loading. However, this condition is valid in the case of flyer plates which do not experience large cycles of recompression once crack propagation begins in the target plate.

5. Comparative study of Effective Moduli model to FDEM simulations and experimental results

5.1. 1D and 2D flyer plate simulations using effective moduli

To test and validate the effective moduli constitutive model as implemented in FLAG, we first simulated the Be-Be flyer plate in both 1D and 2D. The 1D flyer plate FLAG simulation is set up as follows. The impactor and target plates are divided into 26 and 53 zones along their respective thicknesses (Figure 5(a)). A slideline boundary condition is placed in between the plates to allow for a discontinuous mesh and to avoid interpenetration of the two bodies. The impactor is given an initial velocity, v. When the target plate is impacted a compressive shock wave is transferred through the material until it reaches and is reflected off the back side of the plate. When the reflected wave crosses the compressive shockwave a region of high tensile stress is created that causes the target plate to fracture. It is assumed that during the initial compressive regime the cracks in the target plate are unable to grow. Therefore, the moduli of the target plate is not degraded until a tensile stress is present inside the plate. Velocity data at the rear center of the target plate is collected over time for comparison to HOSS simulations and experimental Velocity Interferometer for Any Reflector (VISAR) data (Cady et al., 2012). Figure 5(b) is a comparison of the velocity over time estimation produced by the effective moduli 1D FLAG simulation with a FLAG simulation without a damage model, a high-fidelity HOSS simulation, and experimental data. It can be seen that the hydrodynamics simulation is able to accurately match the first half of the HOSS simulation and experimental VISAR data without a damage model. However, it is unable to match the pull back region of the VISAR curve, depicted in Figure 5(c). In this case, the effective moduli model in FLAG is informed with statistics from one randomly selected HOSS simulation. It was found that the root mean squared error (RMSE) between the effective moduli model and the experimental data was 0.00213 while the RMSE between the effective moduli model and HOSS was 0.00382. The effective moduli model matches the trend of the HOSS results more closely than the experimental VISAR, which is to be expected since the HOSS simulation is directly informing the damage degradation in FLAG. Yet, the 1D FLAG simulation closely approximates the experimental data. The simulation run time for the 1D simulation is FLAG is approximately 42 seconds on one processor, which is a vast reduction in computational resources when compared to the high-fidelity simulations. However, 1D simulations are unable to capture some of the physical phenomenon associated with crack evolution.

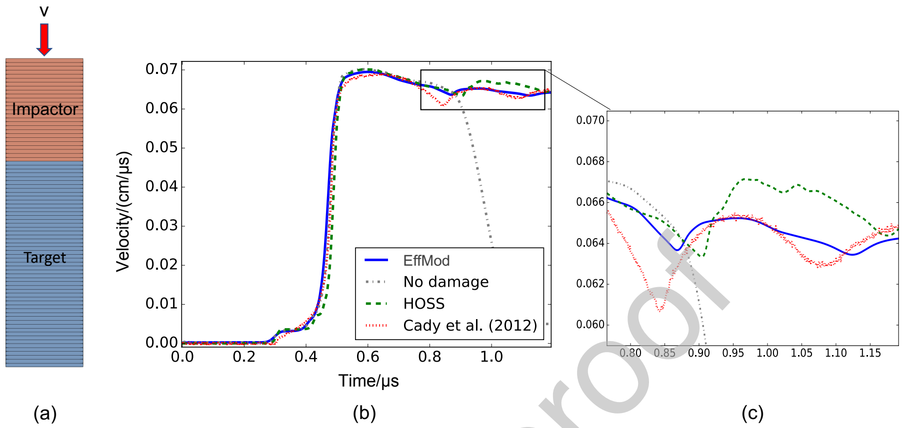

Figure 5: (a) 1D flyer plate simulation setup in FLAG; (b) VISAR comparison of a 1D FLAG simulation with the effective moduli damage model (EffMod) and without a damage model, a HOSS simulation, and experimental data (Cady et al., 2012); and (c) a zoom of the pull back signal

To more accurately capture the physical behavior of the flyer plate experiment, a 2D simulation utilizing the effective moduli model is conducted in FLAG. The flyer plate setup is symmetric about the y-axis thus, in 2D only the left half of the flyer and target plates are modeled to remove extraneous computational expenses. The impactor is divided into 5,184 zones and the target plate is is divided into 10,176 zones, which corresponds to a zone size of approximately $5,625 \mu m^2$. Similar to the 1D case, a slideline boundary is placed in between to two plates to allow for a discontinuous mesh and to avoid interpenetration of the two bodies. Each 2D simulation in FLAG using this setup takes approximately 9 minutes to run on one processor. The 2D FLAG analysis allows for improved visual comparisons of the velocity distributions and spall regions within the target plate over time. Figure 6 depicts the velocity distributions within the impactor and target plates at $t = 1.2 \mu s$. The high-fidelity HOSS simulation clearly shows a complex crack network that forms a wide spall region in the center of the target plate. The FLAG simulation is unable to capture the individual cracks spanning the mid-plane of the target plate; however, a spall region of similar thickness is observed when using the effective moduli model. The spall region in the FLAG simulation is comprised of highly degraded and zero strength material zones that mimic the crack network.

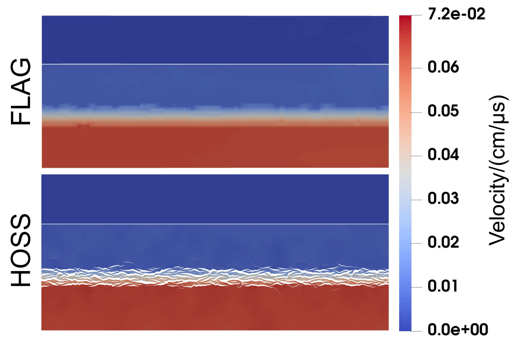

Figure 6: Comparison of the velocity distributions in the FLAG and HOSS flyer plate simulations at $t = 1.2 \mu s$

In the 1D case, results that closely match the HOSS VISAR were generated using crack statistics from a single HOSS simulation. This is in contrast to finding in previous work by Vaughn *et al.* (Vaughn et al., 2019) where a similar modeling approach was used to address low rate uniaxial tensile loading in geo-materials. Vaughn *et al.* (Vaughn et al., 2019) found that statistics from multiple high-fidelity simulations were needed to create a large enough statistical base to qualitatively match experimental results. However, the initial crack distribution considered in these simulations where somewhat limited in comparison to the initial crack network considered here. Their pre-existing crack network consisted of cracks with constant initial lengths and only three possible initial orientations. In addition, there were fewer initial cracks; 20 compared to 200 used here. Having a more varied initial crack network is likely one reason why fewer high-fidelity simulations are needed in this case to generate PDFs that produce reasonable results for the overall material response. The difference in loading conditions may also play a role in the size of the statistical base needed to inform the effective moduli constitutive model. At low rates, a single dominant crack is expected to grow and coalesce, which will engage relatively few cracks in the pre-existing crack network. In the case of high rate loading in a flyer plate experiment, a dominant region of localized damage forms (i.e., the spall region) due to the growth and coalescence of many cracks. In this case, many more cracks in the pre-existing region will be engaged in the formation of a region rather than a single crack pathway.

Regardless of these issues, the initial crack distribution and the crack growth statistics vary from simulation to simulation for the case of a flyer plate. Figure 7(a) shows that the initial rise time is unaffected by variations in the initial crack data but the pull back signals produced after the plate is fractured change from HOSS simulation to HOSS simulation. To investigate the effect the variation in the pre-existing crack network and subsequent statistics have on the pull back signal, we have combined crack length and orientation statistics from 100 HOSS simulations to use to inform the effective moduli constitutive model. The simulated VISAR results, obtained from 2D FLAG simulations, using statistics from two different HOSS simulations as well as statistics from the 100 combined HOSS simulations are presented in Figure 7(b). The variations in the HOSS statistics do not produce significant changes in the VISAR plot produced with the effective moduli in FLAG as can be seen from the inset in Figure 7(b), which is focused on the pull back signal region. This is primarily due to the dense, uniformly distributed initial crack distribution. The initial crack system consists of a large number of short, randomly oriented and distributed cracks. This causes the degraded stiffness tensors and the damage evolution to be nearly identical for every HOSS simulation.

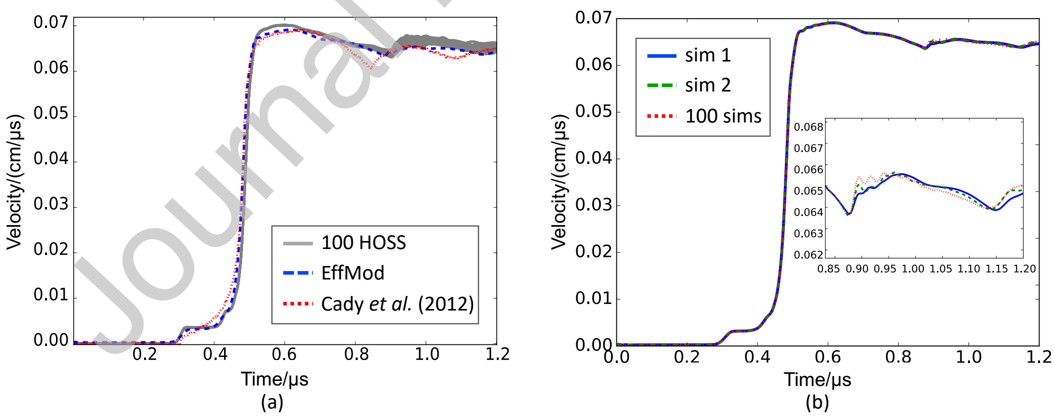

Figure 7: VISARs produced using (a) all 100 HOSS simulations, the effective moduli model in FLAG using statistics from one HOSS simulation, and experimental data from Cady *et al.* (Cady et al., 2012) and (b) the effective moduli model in FLAG using statistics from two different HOSS simulations and averaged statistics from 100 HOSS simulations

5.2. *Effect of the damage threshold on crack evolution statistics*

As stated in Section 2, crack growth in HOSS occurs when the cohesive points between element edges separate until a critical point where these points are broken. In HOSS, a damage value, D_{HOSS}, between 0 and 1 is assigned to each element edge depending on the extent of the separation between cohesive points. $D_{HOSS} = 1$ meaning cohesion between the element edges is completely broken. The crack evolution statistics are highly dependent on the choice of a damage threshold value where cracks are considered to begin opening. In previous sections, a damage threshold value of $D_{HOSS} = 0.1$ was used to determine the crack evolution Figure 8(a) depicts the change in the C_{22} component of the stiffness tensor over time for various values of D_{HOSS}. Cracks form and spread very quickly across the length of the target plate resulting in material failure. The sudden drop-off of the C_{22} component near $t = 0.8\mu s$, corresponds with the fracture of the target plate. Clearly, choosing a higher damage value causes the damage accumulation to become more gradual which corresponds to slower crack growth, an increase in the time it takes for fracture to occur, and a less spontaneous material failure.

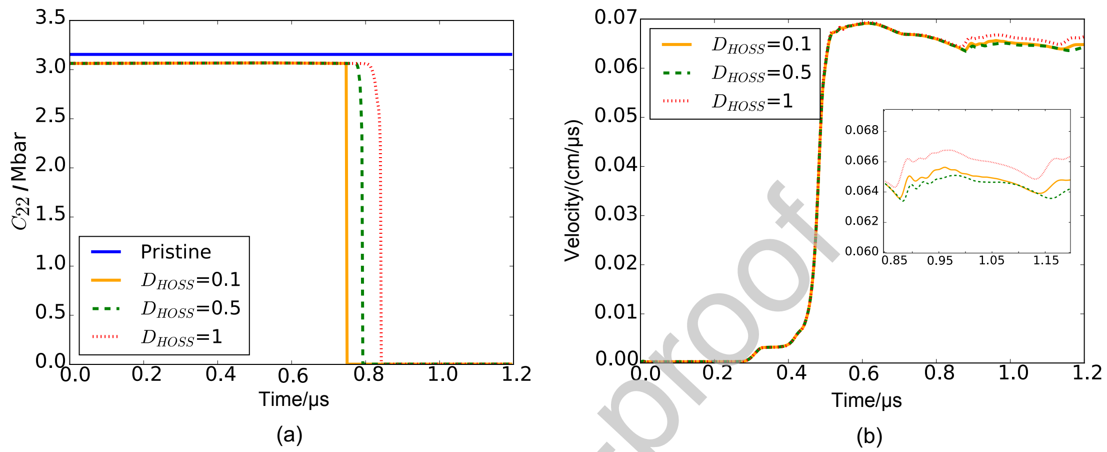

Figure 8: (a) Statistical evolution of the C_{22} component of the stiffness tensor for various HOSS damage thresholds over time compared with the pristine ,undamaged stiffness value, (b) shows the resulting VISAR plots generated using FLAG

While there is very little effect on the velocity data for the various damage thresholds, there is an observable change in the crack evolution and spall region present in the target plate. Figure 9 depicts the damage distributions at the end of simulation $t = 1.2\mu s$, for the various damage thresholds. As D_{HOSS} is increased, the width of the spall region remains approximately the same. However, the spall region becomes more featured and contains a higher number of partially degraded zones. Most notably when $D_{HOSS} = 1$ the outside edges of the spall region experience more of a damage gradient rather than a hard transition from fully damaged zones to slightly degraded zones observed when $D_{HOSS} = 0.1$. The damage distribution resulting from higher values of D_{HOSS} is more reminiscent of experimental behavior.

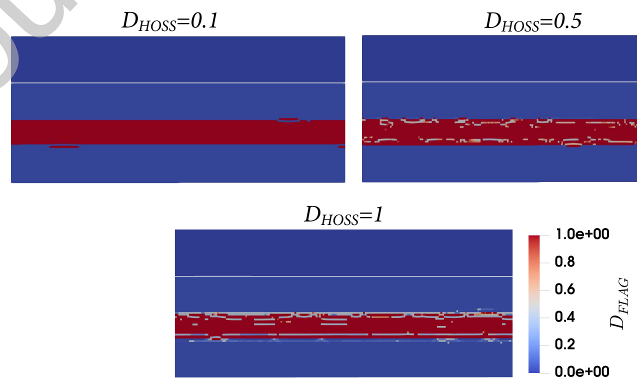

Figure 9: Damage in FLAG at $t = 1.2\mu s$ using sets of statistics formed using various HOSS damage thresholds

5.3. *Model extrapolation for higher velocity flyer plate cases*

A primary goal of this work is to develop a model that can be used generally. Of course, if many high-fidelity simulations are required for every loading condition or each time a new material is employed, the computational cost of generating the needed statistical input could be a major limitation of the methodology presented here. Previously, in Section 5.2, we have shown that one high-fidelity simulation generates enough statistics to produce reasonable results describing the overall material response. However, considering all possible loading conditions and materials one may be interested in studying, requiring a single high-fidelity simulation for each case to inform the crack length and orientation PDFs could still be a significant model limitation.

Cady *et al.* (Cady et al., 2012) also presented experimental data of a Be-Be flyer plate with a higher impact velocity, $v = 0.1246 cm/\mu s$, and the same experimental set-up. We performed simulations at this higher impact velocity using the effective moduli model as implemented in FLAG, but informed with crack length and orientation statistics from a single HOSS simulation modeling the Be-Be flyer plate experiment with an impact velocity of $v = 0.721 cm/\mu s$. Simulated VISAR results are directly compared to the experimental data in Figure 10. The simulated and experimental VISARs match reasonably well, however under closer investigation (see inset in Figure 10) the match is not as good as for the lower velocity case. When the results of the 2D flyer plate simulations in FLAG are compared with the experimental results RMSE the lower rate case was found to be 0.00150 while a RMSE of 0.00202 was found for the extrapolated case. It is to be expected that there would be larger error in the extrapolated response. However, the ability of the effective moduli model to accurately simulate higher velocity flyer plate cases demonstrates that relationship between the maximum tensile stress and damage is similar for Be-Be flyer plates with the same boundary conditions. The ability to extrapolate, with reasonable comparison to experiments, further decreases the need for additional costly high-fidelity simulations to generate statistical input.

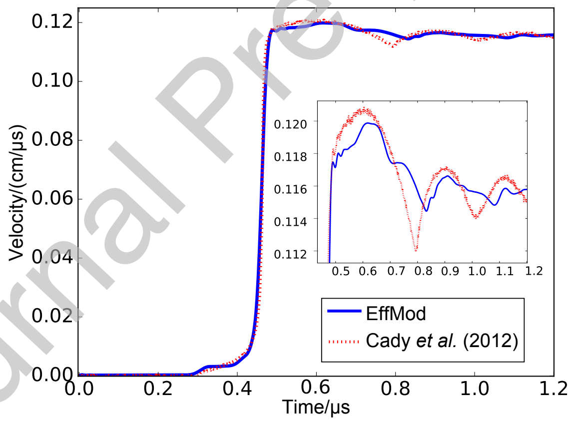

Figure 10: Extrapolation of higher rate flyer plate case compared to experimental results from Cady *et al.* (Cady et al., 2012), considering $D_{HOSS} = 1$ and using statistical data from one HOSS simulation

6. Conclusions

In this work, well defined crack length and orientation statistics from high-fidelity simulations were used to inform an effective moduli model for the high-rate fracture of quasi-brittle metals. A new stress based damage criteria was introduced to allow damage to evolve in individual material zones. This crucial improvement removes the previous limitations associated with the time based damage evolution previously employed by the effective moduli model. Stress based material degradation of individual zones also allows for non-homogeneous damage distributions to form within the material. Thus, realistic regions of localized damage, such as spall regions in the flyer plate experiments simulated in this study, can now be accurately simulated in continuum scale with the effective moduli model. Another important modification to the effective moduli model was the integration of a plasticity model. This allows a wider range of materials, including quasi-brittle materials that exhibit some ductile behavior, can be more accurately simulated.

The effect of variations in the crack statistics was investigated by first studying the number of high-fidelity simulations that were needed to properly inform the damage model. The dense, randomly distributed and oriented pre-existing crack network in the high-fidelity simulations coupled with the indirect tensile loading regime within target plate, lead to very little variation in the crack evolution from simulation to simulation. It was concluded that, one high-fidelity simulation produced adequate statistical information for accurate simulations of the damage evolution with the effective moduli model. This substantially reduces the number of costly high-fidelity simulations needed to create a statically representative set of crack length and orientation distributions. Next the effect of the damage threshold was found to significantly change the damage evolution within the material over time. Higher damage thresholds produced a more gradual material degradation and a later time of failure as well as a more realistic final damage distribution within the target plate. Finally, the effective moduli model was used to extrapolate results for a higher rate loading case. Excellent agreement between experimental results and extrapolated data from the effective moduli model shows that similar stress and crack growth trends are present in the same material at different loading rates. This extension of the effective moduli to higher rate cases further reduces the need for a large number of costly high-fidelity simulations and increases the flexibility of the model.

In future studies, the effective moduli model could be applied and extended to consider more complex loading conditions to include shear loading, combined shear and tension, and recompression of damaged zones. Finally, the model framework is ideal to connect with newly developed reduced-order models, such as those that utilize machine learning (Moore et al., 2018; Hunter et al., 2019). This could also produce more flexibility in the range of statistical information available to inform the constitutive model at greatly reduced computational costs.

7. Acknowledgments

The authors would like to acknowledge Los Alamos National Laboratory Directed Research and Development (LDRD) Program #20170103DR for their financial support.

8. References

Declaration of interests

The authors declare that they have no known competing financial interests or personal relationships that could have appeared to influence the work reported in this paper.

Author Statement

Kevin Larkin: Methodology, Software, Formal analysis, Writing-Original Draft Esteban Rougier: Methodology, Formal Analysis, Writing- Review, & Editing Viet Chau: Methodology, Writing- Review, & Editing Gowri Srinivasan: Conceptualization, Supervision, Writing- Review, & Editing Abdessattar Abdelkefi: Supervision, Writing- Review, & Editing Abigail Hunter: Conceptualization, Supervision, Methodology, Writing- Review, & Editing

References

Abedi, R., Haber, R. B., Clarke, P. L., 2017. Effect of random defects on dynamic fracture in quasi-brittle materials. International Journal of Fracture 208, 241–268.

Abraham, F. F., Broughton, J. Q., Bernstein, N., Kaxiras, E., 1998. Spanning the continuum to quantum length scales in a dynamic simulation of brittle fracture. Europhysics Letters 44, 783.

Addessio, F., Johnson, J. N., 1990. A constitutive model for the dynamics response of brittle materials. Journal of Applied Physics 67, 3275–3286.

Aida, T., Walter, J. W., Aslam, T. D., Short, M., 2013. Verification of 2-d detonation shock dynamics in conjunction with los alamos lagrangian hydrocode. Tech. Rep. LA-UR-12-20792, Los Alamos National Lab, Los Alamos, NM, USA.

Ambati, M., Gerasimov, T., De Lorenzis, L., 2015. A review on phase-field models of brittle fracture and a new fast hybrid formulation. Computational Mechanics 55, 383–405.

Ayyagari, R. S., Daphalapurkar, N. P., Ramesh, K. T., 2018. The effective compliance of spatially evolving planar wing-cracks. Journal of the Mechanics and Physics of Solids 111, 503–529.

BaÅant, Z. P., Caner, F. C., Adley, M. D., Akers, S. A., 2000. Fracturing rate effect and creep in microplane model for dynamics. Journal of Engineering Mechanics, ASCE 126, 962–970.

Blumenthal, W., Abeln, S. P., Cannon, D. D., Gray III, G. T., Carpenter, R. W., 1998. Influence of strain rate and temperature on the mechanical behavior of beryllium. Shock Compression of Condensed Matter 429, 411– 414.

Budiansky, B., O'Connell, R. J., 1976. Elastic moduli of a cracked soild. International Journal of Solids and Structures 12, 81–97.

Burton, D., 1992. Connectivity structures and differencing techniques for staggered-grid free-lagrange hydrodynamics. Tech. Rep. UCRL-JC-110555, Lawrence Livermore National Laboratory, Livermore, CA.

Burton, D., 1994a. Consistent finite-volume discretization of hydrodynamic conservation laws for unstructured grids. Tech. Rep. UCRL-JC-118788, Lawrence Livermore National Laboratory, Livermore, CA.

Burton, D., 1994b. Multidimensional discretization of conservation laws for unstructured polyhedral grids. Tech. Rep. UCRL-JC-118306, Lawrence Livermore National Laboratory, Livermore, CA.

Burton, D., Morgan, N., Charest, M., Kenamond, M., Fung, J., 2018. Compatible, energy conserving, bounds preserving remap of hydrodynamic fields for an extended ale scheme. Journal of Chemical Physics 355, 492–533.

Cady, C. M., Adams, C. D., Prime, M. B., Hull, L. M., Addessio, F. L., Bronkhorst, C. A., Brown, E. N., Liu, C., Sisneros, T. A., Brown, D. W., Blumenthal, W. R., Gray III, G. T., 2012. Characterization of s200-f beryllium using shock loading and quasi-static experiments. Tech. Rep. LA-UR-11-06976, Los Alamos National Laboratory, Los Alamos, NM.

Caldwell, W. K., Hunter, A., Plesko, C. S., Wirkus, S., 2018. Verification and validation of the flag hydrocode for impact cratering simulations. Journal of the American Ceramic Society 3 (3), 031004.

Camacho, G. T., Ortiz, M., 1996. Computational modelling of impact damage in brittle materials. International Journal of Solids and Structures 33 (20-22), 2899–2938.

Chen, W. W., Rajendran, A. M., Song, B., Nie, X., 2007. Dynamic fracture of ceramics in armor applications. Journal of the American Ceramic Society 90 (4), 1005–1018.

Cho, S. H., Ogata, Y., Kaneko, K., 2003. Strain-rate dependency of the dynamic tensile strength of rock. International Journal of Rock Mechanics & Mining Sciences 40, 763–777.

Denissen, N. A., Fung, J., Reisner, J. M., Andrews, M. J., 2012. Implementation and validation of the bhr turbulence model in the flag hydrocode. Tech. Rep. LA-UR-12-24386, Los Alamos National Lab, Los Alamos, NM, USA.

Dienes, G. J., Paskin, A., 1987. Molecular dynamic simulations of crack propagation. Journal of Physics and Chemistry of Solids 48, 1015–1033.

Euser, B., Lei, Z., Rougier, E., Knight, E., Frash, L., Carey, J., Viswanathan, H., Munjiza, A., 2018. 3-d finite-discrete element simulation of a triaxial direct-shear experiment. 52nd US Rock Mechanics/Geomechanics Symposium.

Euser, B., Rougier, E., Lei, Z., Knight, E., Frash, L., Carey, J., Viswanathan, H., Munjiza, A., 2019. Simulation of fracture coalescence in granite via the combined finitediscrete element method. Rock Mechanics and Rock Engineering.
URL `https://doi.org/10.1007/s00603-019-01773-0`

Fung, J., Harrison, A. K., Chitanvis, S., Margulies, J., 2013. Ejecta source and transport modeling in the flag hydorcode. Computers & Fluids 83, 177–186.

Gailly, B. A., Espinosa, H. D., 2002. Modelling of failure mode transition in ballistic penetration with a continuum model describing microcracking and flow of pulverized media. International Journal for Numerical Methods in Engineering 54, 365–398.

Godinez, H., Rougier, E., Osthus, D., Lei, Z., Knight, E., Srinivasan, G., 2019. Fourier amplitude sensitivity test applied to dynamic combined finite-discrete element methodsbased simulations. International Journal for Numerical and Analytical Methods in Geomechanics 43, 30–44.
URL `https://doi.org/10.1016/j.ijrmms.2018.03.016.`

Griffith, A. A., 1921. The phenomena of rupture and flow in solids. Philosophical Transactions of the Royal Society of London 221, 163–198.

Hashin, Z., 1988. The differential scheme and its application to cracked materials. Journal of the Mechanics and Physics of Solids 36 (6), 719–734.

Horii, H., Nemat-Nasser, S., 1983. Overall moduli of solids with microcracks: load-induced anisotropy. Journal of the Mechanics and Physics of Solids 31 (2), 155–171.

Horstemeyer, M. F., 2009. Multiscale modeling: a review. In: Practical aspects of computational chemistry. Springer, Dordrecht, pp. 87–135.

Hunter, A., Moore, B., Mudunuru, M., Chau, V., Miller, R., Tchoua, R., Nyshadham, C., Karra, S., O'Malley, D., Rougier, E., Viswanathan, H., Srinivasan, G., 2019. Reduced-order modeling through machine learning and graph-theoretic approaches for brittle fracture applications. Computational Materials Science 157, 87–98.

Ju, J. W., Chen, T. M., 1994a. Effective elastic moduli of two- dimensional brittle solids with interacting microcracks, part i: Basic formulations. Journal of Applied Mechanics 61, 349–357.

Ju, J. W., Chen, T. M., 1994b. Effective elastic moduli of two- dimensional brittle solids with interacting microcracks, part ii: Evolutionary damage models. Journal of Applied Mechanics 61, 358–366.

Ju, J. W., Tseng, K. H., 1992. A three dimensional statistical micromechanical theory for brittle solids with interacting microcracks. International Journal of Damage Mechanics 1, 102–131.

Ju, J. W., Tseng, K. H., 1995. An improved two-dimensional micromechanical theory for brittle solids with randomly located interacting microcracks. International Journal of Damage Mechanics 4, 23–57.

Kachanov, M., 1993. Elastic solids with many cracks and related problems. Advances in Applied Mechanics 30, 259–445.

Knight, E., Rougier, E., Munjiza, A., 2013. Lanl-csm: Consortium proposal for the advancement of hoss. Tech. Rep. LA-UR-13-23409, Los Alamos National Laboratory, Los Alamos, NM.

Kolanz, M., 2001. Introduction to beryllium: uses, regulatory history, and disease. Applied occupational and environmental hygiene 16, 559–567.

Krishnan, K., Sockalingam, S., Bansal, S., Rajan, S. D., 2010. Numerical simulation of ceramic composite armor subjected to ballistic impact. Composites Part B: Engineering 41, 583–593.

Kushch, V. I., Sevostianov, I., Mishnaevsky Jr., L., 2009. Effect of crack orientation statistics on effective stiffness of microcracked solid. International Journal of Solids and Structures 46, 1574–1588.

Lee, J. D., Wang, X. Q., Chen, Y. P., 2009. Multiscale material modeling and its application to a dynamic crack propagation problem. Theoretical and Applied Fracture Mechanics 51, 33–40.

Li, X., Yang, J. Z., Weinan, E., 2010. A multiscale coupling method for the modeling of dynamics of solids with application to brittle cracks. Journal of Chemical Physics 229, 3970–3987.

Lyon, S. P., 1992. Sesame: the los alamos national laboratory equation of state database. Tech. Rep. LA-UR-92-3407, Los Alamos National Laboratory.

Margolin, L. G., 1983. Elastic moduli of a cracked body. International Journal of Fracture 22, 65–79.

Margolin, L. G., 1984. Microphysical models for inelastic material response. International Journal of Engineering Science 22, 1171–1179.

Meyers, M. A., Aimone, C. T., 1983. Dynamic fracture (spalling) of metals. Progress in Materials Science 28, 1–96.

Moore, B., Rougier, E., O'Malley, D., Srinivasan, G., Hunter, A., Viswanathan, H., 2018. Predictive modeling of dynamic fracture growth in brittle materials with machine learning. Computational Materials Science 148, 46–53.

Munjiza, A., 2004. The combined finite-discrete element method. Wiley, New York.

Munjiza, A., Knight, E. E., Rougier, E., 2012. Computational mechanics of discontinua. Wiley, New York.

Munjiza, A., Owen, D. R. J., Bicanic, N., 1995. A combined finite-discrete element method in transient dynamics of fracturing solids. Engineering computations 12, 145–174.

Munjiza, A., Rougier, E., Knight, E. E., 2015. Large strain finite element method: a practical course, 1st Edition. John Wiley and Sons, London.

Osthus, D., Godinez, H. C., Rougier, E., Srinivasan., G., 2018. Calibrating the stress-time curve of a combined finite-discrete elementmethod to a split hopkinson pressure bar experiment. International Journal of Rock Mechanics & Mining Sciences 106, 278–288. URL `https://doi.org/10.1016/j.ijrmms.2018.03.016`

Preston, D. L., Tonks, D. L., Wallace, D. C., 2003. Model of plastic deformation for extreme loading conditions. Journal of Applied Physics 93 (1), 211–220.

Qiu, R. Z., Lin, Y. C., Fang, T. H., 2018. Fatigue crack growth characteristics of fe and ni under cyclic loading using a quasi-continuum method. Beilstein journal of nanotechnology 9, 1000–1014.

Rougier, E., Knight, E., Lei, Z., Munjiza, A., Mustoe, G., Sarg, R., 2013a. Hoss technology overview: Oil and gas. Tech. Rep. LA-UR-13-29117, Los Alamos National Laboratory.

Rougier, E., Knight, E. E., Broome, S. T., Sussman, A., Munjiza, A., 2014. Validation of a three-dimensional finite-discrete element method using experimental results of the split hopkinson pressure bar test. International Journal of Rock Mechanics & Mining Sciences 70, 101–108.

Rougier, E., Knight, E. E., Munjiza, A., 2013b. Lanl-csm: Hoss - munrou technology overview. Tech. Rep. LA-UR-13-23422, Los Alamos National Laboratory.

Rudd, R. E., Broughton, J. Q., 1998. Coarse-grained molecular dynamics and the atomic limit of finite elements. Physical Review B 58, R5893.

Saadati, M., Forquin, P., Weddfelt, K., Larsson, P. L., 2016. On the tensile strength of granite at high strain rates considering the influence from preexisting cracks. Advances in Materials Science and Engineering 2016.

Saksala, T., Brancherie, D., Harari, I., Ibrahimbegovic, A., 2015. Combined continuum damageembedded discontinuity model for explicit dynamic fracture analyses of quasibrittle materials. ijnme 101.

Sheng, Y., Zeng, X. G., 2016. The deformation mechanisms in process of crack propagation for alpha titanium with compounding microdefects. Advances in Materials Science and Engineering 2016.

Silling, S. A., Askari, E., 2005. A meshfree method based on the peridynamic model of solid mechanics. Computers & Structures 83, 1526–1535.

Simo, J., Hughes, T., 2006. Computational Inelasticity, seventh Edition. Springer Science & Business Media, New York, NY.

Steinberg, D. J., 1996. Equation of state and strength properties of selected materials. Tech. Rep. UCRL-Ma-10639, Lawrence Livermore National Laboratory.

Steinberg, D. J., Cochran, S., Guinan, M., 1980. A constitutive model for metals applicable at high-strain rate. Journal of Applied Physics 51 (3), 1498–1504.

Tadmor, E. B., Ortiz, M., Phillips, R., 1996. Quasicontinuum analysis of defects in solids. Philosophical Magazine A 73, 1529–1563.

Tonks, D. L., Paisley, D. L., Peralta, P. D., Greenfield, S. R., Byler, D. D., Luo, S., Swift, D. C., Koskelo, A. C., 2007. Spallation damage in copper with columnar grains. AIP Conference Proceedings 955, 605–608.

Vaughn, N., A., K., Moore, B., Viswanathan, H., Hunter, A., 2019. Statistically informed upscaling of damage evolution in brittle materials. Theoretical and Applied Fracture Mechanics 102, 210–221.

Xu, T., Fan, J., Stewart, R., Zeng, X., Yao, A., 2017. Quasicontinuum simulation of brittle cracking in singlecrystal material. Crystal Research and Technology 52, 1600247.

Zhou, X., Chen, L., 2018. Review on multi-scale simulation methods. IOP Conference Series: Materials Science and Engineering 394, 032139.

Zi, G., Belytschko, T., 2003. New cracktip elements for xfem and applications to cohesive cracks. International Journal for Numerical Methods in Engineering 57, 2221–2240.

Zimmerman, R. W., 1985. The effect of microcracks on the elastic moduli of brittle materials. Journal of Materials Science Letters 4, 1457–1460.

Zubelewicz, A., Rougier, E., Ostoja-Starzewski, M., Knight, E. E., Bradley, C., Viswanathan, H. S., 2014. A mechanisms-based model for dynamic behavior and fracture of geomaterials. International Journal of Rock Mechanics & Mining Sciences 72, 277–282.